Int. J. Oral Maxillofac. Surg. 2021; 50: 1386–1393
https://doi.org/10.1016/j.ijom.2021.01.003, available online at https://www.sciencedirect.com

International Journal of Oral & Maxillofacial Surgery

Research Paper
Imaging

Registration of magnetic resonance and computed tomography images in patients with oral squamous cell carcinoma for three-dimensional virtual planning of mandibular resection and reconstruction

M. Polfliet[1,2,3], M. S. Hendriks[4], J.-M. Guyader[3,5], I. ten Hove[4], H. Mast[4], J. Vandemeulebroucke[1,2], A. van der Lugt[6], E. B. Wolvius[4], S. Klein[3]

[1]Department of Electronics and Informatics (ETRO), Vrije Universiteit Brussel (VUB), Brussels, Belgium; [2]imec, Leuven, Belgium; [3]Biomedical Imaging Group Rotterdam, Departments of Medical Informatics and Radiology, Erasmus University Medical Center, Rotterdam, The Netherlands; [4]Department of Oral and Maxillofacial Surgery, Erasmus University Medical Center, Rotterdam, The Netherlands; [5]LabISEN – Yncréa Ouest, Brest, France; [6]Department of Radiology and Nuclear Medicine, Erasmus University Medical Center, Rotterdam, The Netherlands

M. Polfliet, M. S. Hendriks, J. -M. Guyader, I. ten Hove, H. Mast, J. Vandemeulebroucke, A. van der Lugt, E. B. Wolvius, S. Klein: Registration of magnetic resonance and computed tomography images in patients with oral squamous cell carcinoma for three-dimensional virtual planning of mandibular resection and reconstruction. Int. J. Oral Maxillofac. Surg. 2021; 50: 1386–1393.

Abstract. The aim of this study was to evaluate and present an automated method for registration of magnetic resonance imaging (MRI) and computed tomography (CT) or cone beam CT (CBCT) images of the mandibular region for patients with oral squamous cell carcinoma (OSCC). Registered MRI and (CB)CT could facilitate the three-dimensional virtual planning of surgical guides employed for resection and reconstruction in patients with OSCC with mandibular invasion. MRI and (CB)CT images were collected retrospectively from 19 patients. MRI images were aligned with (CB)CT images employing a rigid registration approach (stage 1), a rigid registration approach using a mandibular mask (stage 2), and two non-rigid registration approaches (stage 3). Registration accuracy was quantified by the mean

0901-5027/01001386 + 08

target registration error (mTRE), calculated over a set of landmarks annotated by two observers. Stage 2 achieved the best registration result, with an mTRE of 2.5 ± 0.7 mm, which was comparable to the inter- and intra-observer variabilities of landmark placement in MRI. Stage 2 was significantly better aligned compared to all approaches in stage 3. In conclusion, this study demonstrated that rigid registration with the use of a mask is an appropriate image registration method for aligning MRI and (CB)CT images of the mandibular region in patients with OSCC.

Key words: oral squamous cell carcinoma; mandibular reconstruction; X-ray computed tomography; magnetic resonance imaging; multimodal imaging; medical image processing.

Accepted for publication 4 January 2021
Available online 5 February 2021

Oral squamous cell carcinoma (OSCC) is the sixth most common cancer worldwide. The overall 5-year survival rate of patients with OSCC is less than 50% and has not shown any significant improvement over the last decades, despite advances in treatment modalities[1–5].

Segmental mandibular resection and reconstruction with a free vascularized osseocutaneous flap is currently the recommended treatment for OSCC invading the mandible[6]. The main goal of surgical treatment is to obtain tumour-free resection margins with acceptable remaining function (chewing, swallowing, and speaking) and physical appearance. Achieving tumour-free resection margins is challenging, but crucial for disease control and survival[1,3,7–12]. Recent studies reported that inadequate resection margins were found in 20% of the bone resections, which negatively impacted the 5-year survival rate of patients[1,3,7]. The inability to distinguish tumour from healthy bone tissue intraoperatively during resection is the most common cause of such inadequate margins[10]. Additionally, a re-resection of positive margins in a second operation is not desirable due to technical difficulties, and has a negative effect on the survival of the transplant[11]. During resection, tumour-free surgical margins are the only prognostic factor that the surgeon can control[11].

The state-of-the-art mandibular reconstruction method is based on preoperative three-dimensional (3D) virtual surgical planning using 3D-printed surgical guides[12–14]. With this method, the patient undergoes the necessary imaging, after which the surgeon virtually defines the cutting planes and plans the resection and subsequent reconstruction. Thereafter, the surgical guides are printed and the virtual planning is translated to the surgical procedure. Cutting guides for the mandible and fibula have been shown to provide a better fit of the fibula parts, resulting in a reduced surgical time. However, accurate 3D virtual planning of the surgical cutting guides remains essential in order to achieve a complete resection.

Current 3D virtual planning is based on computed tomography (CT) or cone beam CT (CBCT) images, which offer detailed information on bone geometry and cortical bone destruction, but do not provide accurate information on bone marrow involvement and perineural spread of the tumour. In recent years, magnetic resonance imaging (MRI) has increasingly been used for diagnostic purposes due to its better visualization of tumour tissue, mandibular bone marrow involvement, and perineural spread along the inferior alveolar nerve[3,15–17].

The uncertainty about the location of the tumour boundaries in the 3D virtual planning based on (CB)CT acquisitions could be eliminated by including MRI aquisitions[18]. Overlaying or fusing these MRI and (CB)CT images before the preoperative virtual planning could aid the surgeon in defining the surgical guides and subsequent reconstruction through a more accurate determination of the osteotomy location and a better understanding of the surrounding structures. The integration of fused CT and MRI images for mandibular resection planning in clinical practice has been shown to be a safe and accurate alternative[19]. However, due to the different orientation and position of the mandible in the MRI and (CB)CT acquisitions, an image registration method is required to establish the spatial correspondences between the different images.

The aim of this study was to evaluate and present an automated method to perform image registration of MRI and (CB)CT in the mandibular region in patients with OSCC, which could subsequently be integrated into a pipeline for the virtual planning of mandibular resections and reconstructions.

Materials and methods

Dataset

The study was reviewed and approved by the local medical ethics review committee (MEC-2016-143) and was performed in accordance with national and international legislation. The need for informed consent was waived owing to the retrospective and anonymized nature of the study. Preoperative 3D MRI and (CB)CT scans of the head and neck region were collected retrospectively from 19 patients diagnosed between 2014 and 2016 with untreated primary OSCC with invasion of the mandible. The images were anonymized prior to processing. The MRI scans were acquired with a Spin Echo T1-weighted sequence. The in-plane voxel size of MRI was between 0.4×0.4 mm^2 and 0.5×0.5 mm^2, and slice thickness was between 3 mm and 4 mm. The echo time (TE) ranged from 10.8 ms to 13.6 ms, the repetition time (TR) from 416 ms to 689 ms, and the flip angle (FA) was 90°, 111°, or 160°. The CT imaging in-plane voxel size ranged from 0.3×0.3 mm^2 to 0.5×0.5 mm^2, and slice thickness from 0.3 mm to 0.6 mm. The CBCT imaging in-plane voxel size was 0.3×0.3 mm^2 and slice thickness was 1 mm. The mean time between the MRI and (CB)CT scans was 9 days (range 2–23 days, standard deviation (SD) 5.3 days). No pre- or post-processing was applied to the images and they remained unmodified for the registration.

Registration

An automated image registration method to align the MRI with the (CB)CT images was investigated. The alignment was achieved in three stages. In the first stage, an initial rigid alignment was estimated. Thereafter a more refined rigid alignment was estimated, focused around the mandible. In the third and final stage, a deformable alignment was performed, for which different approaches were compared. In all stages, an automated intensity-based 3D registration framework (Elastix)[20] was used, based on the maximization of mutual information[21] using a stochastic gradient descent optimization method[22].

In the first stage, two consecutive registrations were performed to achieve an initial rigid alignment. First, a global translation was estimated, since the MRI images needed to be roughly aligned to the

(CB)CT image domain. Subsequently, a rigid registration was conducted, estimating both translations and rotations (parameterized by Euler angles).

In the second stage, the initial rigid alignment was fine-tuned by restricting the focus of the algorithm on a 3D region of interest encompassing the mandible, manually drawn in the (CB)CT image. As such, all image information outside of the region of interest was ignored and potential registration difficulties due to pose or appearance changes could be alleviated. The mandibular mask was drawn slice by slice, using open-source ITK-SNAP software[23].

In the third stage, an evaluation was performed to determine whether the alignment could be refined further using a non-rigid (or deformable) registration to compensate for any geometric distortions in the MRI images[24]. A parametric B-spline free-form deformation model was employed, and (isotropic) control point spacings of 64 mm, 32 mm, and 16 mm were evaluated[25]. Furthermore, two different approaches for the deformable registration were compared: (a) an asymmetric approach with the (CB)CT image as the fixed (or target, reference) image and the MRI as the moving (or template, source) image; and (b) a symmetric approach in which both images were registered to a common mid-space[26]. Results from the literature suggest that symmetric registration techniques can lead to improved registration accuracy and inverse-consistency[27,28], which are especially critical for treatment planning[29].

All stages are illustrated in Fig. 1. The three registration stages were executed in a consecutive manner. The registration result after stage 1 was employed to initialize the registration in stage 2. The registration result after stage 2 was employed to initialize the registration in stage 3, where either approach 3a or approach 3b was taken.

Evaluation

Registration accuracy in the mandibular region was evaluated in terms of the mean target registration error (mTRE), by computing the Euclidean distance between corresponding landmarks in MRI and (CB)CT and then averaging it over all landmarks[30]. An extensive landmark set was designed with 39 anatomical reference points in order to evaluate the registration error for the entire mandible specifically. The set consisted of 22 landmarks placed at the roots of each lower tooth (for the molars, both roots were considered as landmarks) and 17 anatomical reference points on the mandible. The set of landmarks is described in detail in Table 1 and Fig. 2. Due to tumour invasion in the bone or removed tooth elements, not all landmarks from the dataset could be annotated for all images.

The landmarks were annotated manually in each MRI and (CB)CT acquisition by

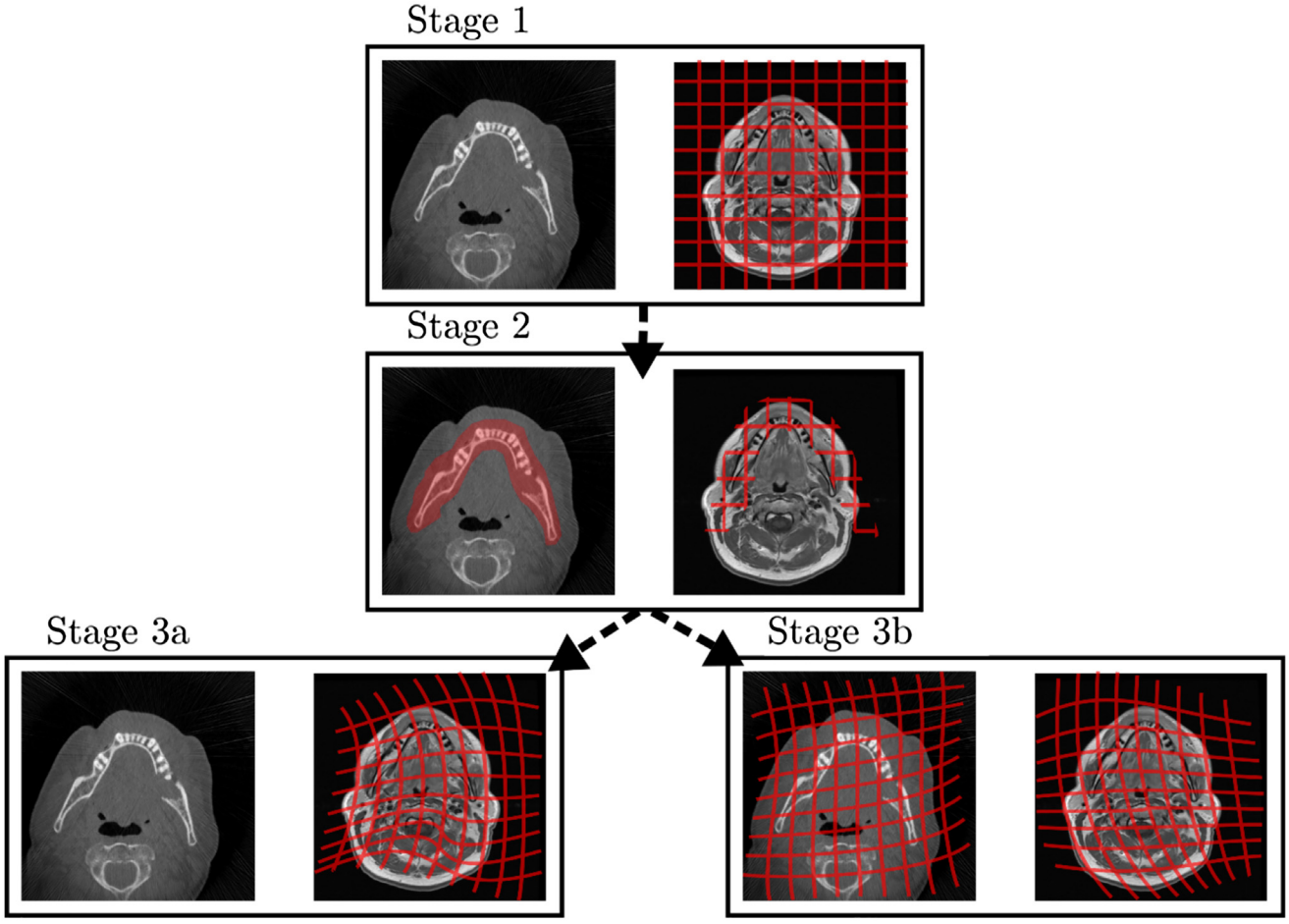

Fig. 1. The proposed three-stage registration method to align MRI with (CB)CT images in the mandibular region. In the first stage, an initial rigid alignment was estimated. Thereafter, in the second stage, a more refined rigid alignment focused around the mandible was estimated. In the third (and final) stage, two approaches for deformable alignment were investigated side by side: an asymmetric (3a) and a symmetric approach (3b). Note that, unlike the schematic 2D illustrations in this figure, all registrations were performed completely in the 3D space.

Table 1. Description of the anatomical landmarks on the teeth and the mandible.

Abbreviation	Landmark	Description
t31, t32, t33, t34, t35, t36, t37, t38, t41, t42, t43, t44, t45, t46, t47, t48	Teeth of the third and fourth quadrants	22 landmarks on the teeth; the molars (36, 37, 38, 46, 47, 48) have two roots
A	Menton	The most inferior point of the mandibular symphysis
B	Mental foramen	Foramen located on the anterior side of the mandible
C	Gonion	A point defined as the mandibular angle, representing the intersection of the lines of the posterior ramus and the inferior border of the mandible
D	Mandibular foramen	Foramen located on the internal surface on the ramus
E	Coronoid process	The tip of the coronoid process
F	Left condylion	Leftmost aspect of the condylar head
G	Right condylion	Rightmost aspect of the condylar head
H	Top condylion	Top of the condylar head
I	Mandibular notch	Notch located at the most superior point of the ramus, which separates the coronoid process anteriorly and the condyloid process posteriorly

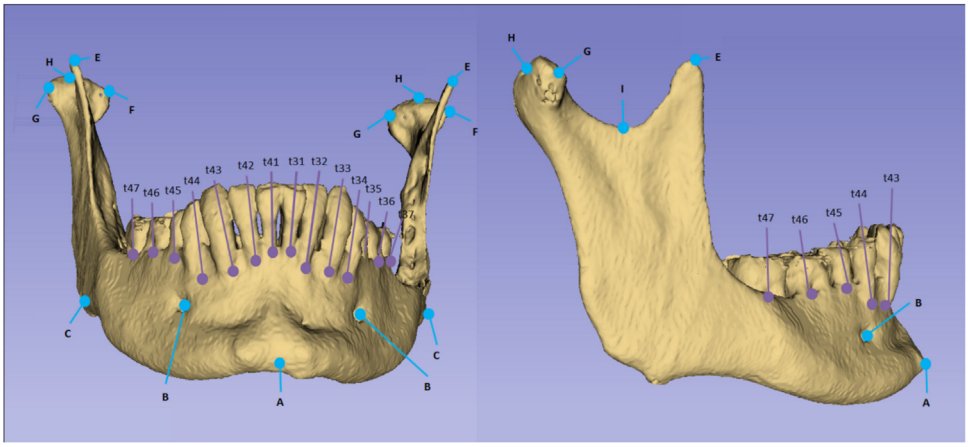

Fig. 2. Tooth and mandibular evaluation landmarks. The purple and blue landmarks indicate the apices of the teeth and the anatomical positions of the mandible, respectively. These 39 landmarks correspond with the landmarks described in Table 1. Landmark D is not illustrated in this figure, because this landmark is behind the field of view. Landmarks t38 and t48 were not present in this subject. Note that the 3D model shown here was generated for illustration purposes only; during annotation of the landmarks, the original (CB)CT and MRI acquisitions were used, inspecting image slices in three orthogonal planes (axial, sagittal, coronal).

two researchers (M.S.H., J.-M.G.) who were trained in advance. The reliability of each landmark was investigated by calculating the inter-observer variability for both MRI and (CB)CT images separately. In addition, one observer (M.S.H.) repeated the annotation of all landmarks, to enable the assessment of the intra-observer variability. Intra- and inter-observer variability were quantified by calculating the Euclidean distance (similar to the mTRE) between corresponding landmarks of the same and different observer, respectively.

If the inter-observer variability for a landmark was greater than 5 mm, the landmark was excluded (when applicable both for left and right sides). After the exclusion of the unreliable landmarks, the mTRE was calculated for each registration stage to assess the registration accuracy.

Statistical analysis

Two statistical analyses were performed. First, a comparison was made between the stage that performed best (with the lowest mTRE) and all other registration stages. Second, for the third stage a comparison was made between the asymmetric and symmetric approach for each spacing of the control points (64 mm, 32 mm, and 16 mm). A two-sided Wilcoxon signed rank test at a significance level of 0.05 was used to evaluate the differences in the distribution of the mTRE.

Results

The inter-observer variability for the landmarks gonion (C) and coronoid process (E) was greater than 5 mm (6.5 mm and 6.0 mm, respectively). These landmarks on both sides of the mandible were therefore excluded from the calculation of the mTRE and the observer variabilities. On average, 20 landmarks per patient remained to calculate the mTRE.

The inter-observer variability and intra-observer variability (mean $\pm$ SD over all subjects) for landmark placement were found to be 2.4 ± 0.7 mm and 2.0 ± 0.5 mm, respectively, for MRI images and 1.5 ± 0.8 mm and 1.0 ± 0.3 mm, respectively, for (CB)CT images.

After rigid registration in stage 1, the mTRE (mean $\pm$ SD over all subjects) was 3.1 ± 1.8 mm. After rigid registration with the use of a mask around the mandible (stage 2), the mTRE was 2.5 ± 0.7 mm. After asymmetric non-rigid registration (stage 3a) with B-spline control point spacings of 64 mm,

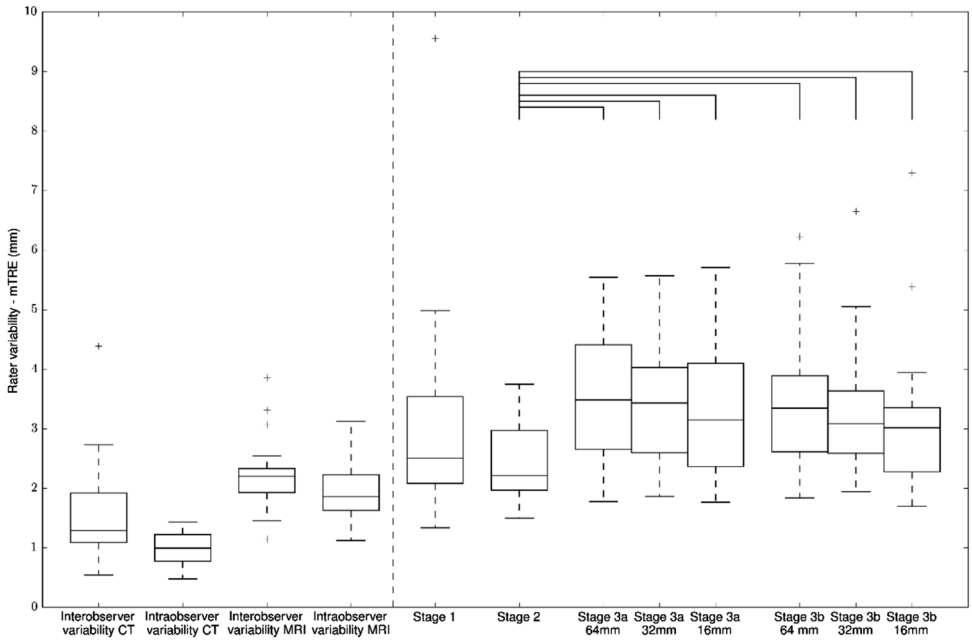

Fig. 3. Boxplots representing the distributions of the inter- and intra-observer variabilities for CT and MRI and of the mTRE values for each registration stage. The square brackets between two connected boxplots indicate statistical significance at a level of 0.05.

32 mm, and 16 mm, the mTREs were 3.6 ± 1.1 mm, 3.4 ± 1.1 mm, and 3.3 ± 1.2 mm, respectively. In the symmetric non-rigid registration (stage 3b), the mTRE values were found to be 3.5 ± 1.2 mm, 3.3 ± 1.2 mm, and 3.1 ± 1.3 mm, respectively. Fig. 3 shows the distributions of mTRE over all subjects for each registration stage, as well as the inter- and intra-observer variability.

Compared to stage 2, which yielded the lowest average mTRE, stage 3 produced significantly different mTRE values (3a, 64 mm: $W = 5$, $P < 0.001$; 3a, 32 mm: $W = 2$, $P < 0.001$; 3a, 16 mm: $W = 6$,

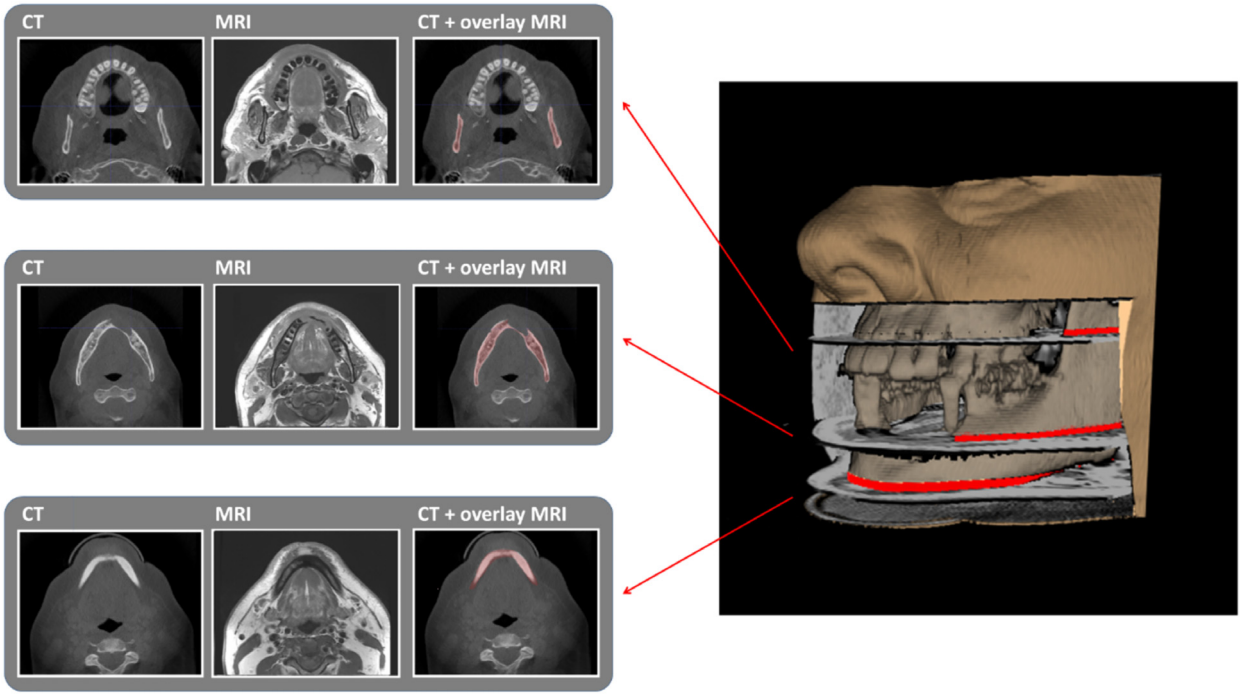

Fig. 4. This figure illustrates the result of the registration of MRI and CT images after stage 2 of a representative case (subject 8). The mandible was segmented in the registered MRI images and overlaid in red with the corresponding CT images in three randomly selected slices. These results were combined in a 3D rendering with the segmented skull and mandible from the CT images. The gap at the front represents tumour tissue which is invading the mandible in and around the anterior part of the mandible.

$P < 0.001$; 3b, 64 mm: $W = 3$, $P < 0.001$; 3b, 32 mm: $W = 15$, $P = 0.001$; 3b, 16 mm: $W = 26$, $P = 0.005$). No significant difference was found between stage 1 and stage 2 ($W = 47$, $P = 0.054$) or between stage 3a and stage 3b (64 mm: $W = 59$, $P = 0.147$; 32 mm: $W = 69$, $P = 0.294$; 16 mm: $W = 48$, $P = 0.059$). A representative case illustrating the result of the registration of MRI and CT images after stage 2 is given in Fig. 4.

Regarding the computation time, stage 1 required 266 ± 65 s to complete; stage 2 required an additional 131 ± 37 s. Stage 3a required an additional 285 ± 48 s, 288 ± 34 s, and 294 ± 51 s, for 64 mm, 32 mm, and 16 mm, respectively, whereas in stage 3b these computations required 1138 ± 140 s, 1234 ± 139 s, and 1356 ± 151 s, respectively. All experiments were performed single-threaded on the local university CPU cluster.

Discussion

This study showed that the rigid registration with a mask (stage 2) is the recommended method for registering MRI and (CB)CT images in the mandibular region. Stage 2 achieved a lower mTRE compared to stage 1, although the difference was not significant ($P = 0.054$). However, the localized focus in stage 2 should generalize better to other patients and be more robust to outliers. A protocol for applying the recommended method is provided in the Appendix A.

In this work, two approaches for deformable registration were applied. A conventional asymmetric approach where the (CB)CT image was employed as the fixed image and the MRI image as the moving image (stage 3a) and a symmetric approach where the images were registered to a common reference system (stage 3b). Although the differences were not statistically significant, stage 3b achieved a marginal improvement compared to stage 3a for all control point spacings of 64 mm, 32 mm, and 16 mm. Furthermore, the registration error of all approaches in stage 3 was significantly higher than the error in stage 2. As such, the results indicate that non-rigid registration (stage 3) has no added value in this application.

With the large number of landmarks (35 after the exclusions), the mTRE could be estimated reliably. This was even the case for patients for whom not all landmarks could be annotated, e.g. cases where tooth elements were extracted, cases with bone invasion by tumour, and cases with a landmark outside the field of view. The inter- and intra-observer variability of landmark annotations in the (CB)CT images were consistent with those reported in the literature[31,32]. Furthermore, the mTRE achieved by the best registration method (stage 2, 2.5 mm) was similar to the inter- and intra-observer variabilities for MRI images (2.4 mm and 2.0 mm, respectively). As such, lower mTRE values based on the landmarks employed in this study can hardly be expected. Note that a recent study on landmark accuracy in MRI images found lower inter- and intra-observer variability[33]. However, this difference can be explained by the considerably lower slice thickness employed in that previous study (0.53 mm vs at least 3 mm in the present study). Based on the inter- and intra-observer variabilities, the gonion and coronoid process landmarks were excluded; their annotations were most likely hindered by the poor delineation and fuzzy boundaries of the landmark locations[34]. Of note, several other evaluation methodologies for registration accuracy exist, such as the Euclidean distance between centroids, overlap measures, and surface distances of manually segmented anatomical structures[35,36]. In this study, we opted for manual landmark annotations, since a relatively large number of well-defined landmarks could be identified, allowing a reliable estimation of the mTRE, while manual segmentation would have been much more time-consuming.

It appears that data on the registration of MRI and (CB)CT images of the head and neck region are scarce. Previous studies have found registration errors in the range of 1.7–3.3 mm in datasets of four to 16 patients[37–41]. None of these previous studies focused specifically on the mandible, hindering a thorough comparison with the present study. However, the results of these studies suggest that the mTRE of 2.5 mm (for stage 2) achieved indicates a state-of-the-art error level.

Fortunati et al.[42] suggested that patient immobilization during imaging leads to better registration of the MRI and (CB)CT images of the head and neck region. Their study found a registration error of 7.0 mm without immobilization and a registration error of 1.9 mm with immobilization. The implementation of immobilization equipment for our specific application might not add value in clinical practice, since a competitive mTRE of 2.5 mm was already achieved without immobilization. Moreover, rigorous immobilization of the mandible would be challenging and likely not comfortable for the patient.

The mandibular mask used in stage 2 was drawn manually around the mandible in each slice of the (CB)CT images. Although the mask does not have to be delineated very precisely (it just serves to indicate an approximate region of interest), this manual interaction step may not be desirable in clinical practice. The development of a robust semi-automated or even fully automated segmentation[43] is therefore recommended to accelerate this step. We refer the reader to a recent review of such methodologies for a full overview[44].

Although the open-source Elastix software was used to implement the image registrations in this study, other (open-source or commercial) software applications that implement similar registration algorithms based on maximization of mutual information could have been used as well. Some well-known open-source examples include NiftyReg[45] and ITKv4/ANTS[46]. After proper configuration, these tools are expected to achieve similar registration accuracy.

Correct determination of the osteotomy location depends on several factors (e.g. the waiting time between imaging and surgery, the process of the translation from 3D virtual planning to the patient, the accurate placement of the cutting guide during surgery, the length of the fibula reconstruction, the relationship of the tumour to the mental nerve and the remaining teeth), which could independently contribute to positive resection margins. For example, several studies have shown that CBCT results in less accurate 3D planning models than CT[47]. When the proposed registration method is translated into clinical practice, image registration errors have to be considered in conjunction with all other sources of errors.

No clinical outcome criteria were employed in this work, such as the resection margin, the frequency of revising the surgical guide during planning, or frequency of local tumour progression, as this was a retrospective study. A randomized clinical trial is needed to determine the added value of registered MRI and CB (CT) in virtual planning of mandibular resection and reconstruction.

This study presented an image registration method for aligning MRI and (CB)CT images of the mandibular region in patients with OSCC. It showed that rigid registration within a region of interest drawn around the mandible is the recommended registration method for the alignment of MRI and (CB)CT images in the mandibular region.

Funding

This study was partially funded by Fonds NutsOhra (nr.1404-048).

Competing interests

The authors declare that there is no conflict of interest.

Ethical approval

The study was reviewed and approved by the local medical ethics review committee (MEC-2016-143) and was performed in accordance with national and international legislation.

Patient consent

The need for informed consent was waived owing to the retrospective and anonymized nature of the study.

Appendix A

Protocol

We have made the code to execute the registration available in a public GitHub repository (https://github.com/MathiasLPolfliet/mandible_ct_mri_registration). The protocol can be subdivided into three steps:

1) *Obtain a rough registration mask of the mandible.* The binary registration must overlay the mandible entirely. Furthermore, the mask must have a boundary around the mandible of roughly 16 pixels in all dimensions.
2) *Perform initial rigid registration (stage 1).* Perform a sequential registration, optimizing a translation transformation followed by a translation and rotation, to roughly align the anatomical structures in the acquisitions. Store the resulting transformation to initialize stage 2.
3) *Perform rigid registration with masked field of view (stage 2).* Initialize a new registration with the result from stage 1 and limit the field of view with the binary registration mask. Optimize for the translation and rotation transformation.

References

1. Binahmed A, Nason RW, Abdoh AA. The clinical significance of the positive surgical margin in oral cancer. *Oral Oncol* 2007;**43**:780–4.
2. Carvalho AL, Nishimoto IN, Califano JA, Kowalski LP. Trends in incidence and prognosis for head and neck cancer in the United States: a site-specific analysis of the SEER database. *Int J Cancer* 2005;**114**:806–16.
3. Nieberler M, Häußler P, Kesting MR, Kolk A, Deppe H, Weirich G, Wolff K-D. Clinical impact of intraoperative cytological assessment of bone resection margins in patients with head and neck carcinoma. *Ann Surg Oncol* 2016;**23**:3579–86.
4. Shah JP, Gil Z. Current concepts in management of oral cancer—surgery. *Oral Oncol* 2009;**45**:394–401.
5. Safi AF, Kauke M, Grandoch A, Nickenig HJ, Zöller JE, Kreppel M. Analysis of clinicopathological risk factors for locoregional recurrence of oral squamous cell carcinoma—retrospective analysis of 517 patients. *J Craniomaxillofac Surg* 2017;**45**:1749–53.
6. Succo G, Berrone M, Battiston B, Tos P, Goia F, Appendino P, Crosetti E. Step-by-step surgical technique for mandibular reconstruction with fibular free flap: application of digital technology in virtual surgical planning. *Eur Arch Otorhinolaryngol* 2015;**272**:1491–501.
7. Smits RWH, Ten Hove I, Dronkers EAC, Bakker Schut TC, Mast H, de Jong RJ Baatenburg, Wolvius EB, Puppels GJ, Koljenović S. Evaluation of bone resection margins of segmental mandibulectomy for oral squamous cell carcinoma. *Int J Oral Maxillofac Surg* 2018;**47**:959–64.
8. Kademani D, Bell RB, Bagheri S, Holmgren E, Dierks E, Potter B, Homer L. Prognostic factors in intraoral squamous cell carcinoma: the influence of histologic grade. *J Oral Maxillofac Surg* 2005;**63**:1599–605.
9. Kreppel M, Drebber U, Eich HT, Dreiseidler T, Zöller JE, Müller RP, Scheer M. Combined-modality treatment in advanced oral squamous cell carcinoma: Primary surgery followed by adjuvant concomitant radiochemotherapy. *Strahlenther Onkol* 2011;**187**:555–60.
10. Barroso EM, Ten Hove I, Schut TC Bakker, Mast H, van Lanschot CGF, Smits RWH, Caspers PJ, Verdijk R, Noordhoek Hegt V, Baatenburg de Jong RJ, Wolvius EB, Puppels GJ, Koljenović S. Raman spectroscopy for assessment of bone resection margins in mandibulectomy for oral cavity squamous cell carcinoma. *Eur J Cancer* 2018;**92**:77–87.
11. Dillon JK, Brown CB, McDonald TM, Ludwig DC, Clark PJ, Leroux BG, Futran ND. How does the close surgical margin impact recurrence and survival when treating oral squamous cell carcinoma? *J Oral Maxillofac Surg* 2015;**73**:1182–8.
12. Varvares MA, Poti S, Kenyon B, Christopher K, Walker RJ. Surgical margins and primary site resection in achieving local control in oral cancer resections. *Laryngoscope* 2015;**125**:2298–307.
13. Tarsitano A, Ciocca L, Cipriani R, Scotti R, Marchetti C. Mandibular reconstruction using fibula free flap harvested using a customised cutting guide: how we do it. *Acta Otorhinolaryngol Ital* 2015;**35**:198.
14. Cornelius CP, Giessler GA, Wilde F, Metzger MC, Mast G, Probst FA. Iterations of computer- and template assisted mandibular or maxillary reconstruction with free flaps containing the lateral scapular border—evolution of a biplanar plug-on cutting guide. *J Craniomaxillofac Surg* 2016;**44**:229–41.
15. Li C, Men Y, Yang W, Pan J, Sun J, Li L. Computed tomography for the diagnosis of mandibular invasion caused by head and neck cancer: a systematic review comparing contrast-enhanced and plain computed tomography. *J Oral Maxillofac Surg* 2014;**72**:1601–15.
16. Li C, Yang W, Men Y, Wu F, Pan J, Li L. Magnetic resonance imaging for diagnosis of mandibular involvement from head and neck cancers: a systematic review and meta-analysis. *PLoS One* 2014;**9**:e112267.
17. Blatt S, Ziebart T, Krüger M, Pabst AM. Diagnosing oral squamous cell carcinoma: how much imaging do we really need? A review of the current literature. *J Craniomaxillofac Surg* 2016;**44**:538–49.
18. Dong Y, Dong Y, Hu G, Xu Q. Three-dimensional reconstruction of extremity tumor regions by CT and MRI image data fusion for subject-specific preoperative assessment and planning. *Comput Aided Surg* 2011;**16**:220–33.
19. Kraeima J, Dorgelo B, Gulbitti HA, Steenbakkers RJHM, Schepman KP, Roodenburg JLN, Spijkervet FKL, Schepers RH, Witjes MJH. Multi-modality 3D mandibular resection planning in head and neck cancer using CT and MRI data fusion: a clinical series. *Oral Oncol* 2018;**81**:22–8.
20. Klein S, Staring M, Murphy K, Viergever MA, Pluim JP. Elastix: a toolbox for intensity-based medical image registration. *IEEE Trans Med Imaging* 2010;**29**:196–205.
21. Thévenaz P, Unser M. Optimization of mutual information for multiresolution image registration. *IEEE Trans Image Process* 2000;**9**:2083–99.
22. Klein S, Pluim JP, Staring M, Viergever MA. Adaptive stochastic gradient descent optimisation for image registration. *Int J Comput Vis* 2009;**81**:227–39.
23. Yushkevich PA, Piven J, Hazlett HC, Smith RG, Ho S, Gee JC, Gerig G. User-guided 3D active contour segmentation of anatomical structures: significantly improved efficiency and reliability. *Neuroimage* 2006;**31**:1116–28.
24. Chang H, Fitzpatrick JM. A technique for accurate magnetic resonance imaging in the presence of field inhomogeneities. *IEEE Trans Med Imaging* 1992;**11**:319–29.
25. Rueckert D, Sonoda LI, Hayes C, Hill DL, Leach MO, Hawkes DJ. Nonrigid registration using free-form deformations: applica-

tion to breast MR images. *IEEE Trans Med Imaging* 1999;**18**:712–21.
26. Bhatia KK, Hajnal JV, Puri BK, Edwards AD, Rueckert D. Consistent groupwise non-rigid registration for atlas construction. *Biomedical Imaging: Nano to Macro, 2004*. IEEE International Symposium on Biomedical Imaging. IEEE; 2004: 908–11.
27. Aganj I, Iglesias JE, Reuter M, Sabuncu MR, Fischl B. Mid-space-independent deformable image registration. *Neuroimage* 2017;**152**:158–70.
28. Lorenzi M, Ayache N, Frisoni GB, Pennec X. Alzheimer's Disease Neuroimaging Initiative (ADNI). LCC-Demons: a robust and accurate symmetric diffeomorphic registration algorithm. *Neuroimage* 2013;**81**:470–83.
29. Rivest-Hénault D, Dowson N, Greer PB, Fripp J, Dowling JA. Robust inverse-consistent affine CT–MR registration in MRI-assisted and MRI-alone prostate radiation therapy. *Med Image Anal* 2015;**23**:56–69.
30. Fitzpatrick JM, West JB. The distribution of target registration error in rigid-body point-based registration. *IEEE Trans Med Imaging* 2001;**20**:917–27.
31. Ludlow JB, Gubler M, Cevidanes L, Mol A. Precision of cephalometric landmark identification: cone-beam computed tomography vs conventional cephalometric views. *Am J Orthod Dentofacial Orthop* 2009;**136**. 312. e1–10.
32. Lagravère MO, Low C, Flores-Mir C, Chung R, Carey JP, Heo G, Major PW. Intraexaminer and interexaminer reliabilities of landmark identification on digitized lateral cephalograms and formatted 3-dimensional cone-beam computerized tomography images. *Am J Orthod Dentofacial Orthop* 2010;**137**:598–604.
33. Juerchott A, Freudlsperger C, Zingler S, Saleem MA, Jende JM, Lux CJ, Bendszus M, Heiland S, Hilgenfeld T. In vivo reliability of 3D cephalometric landmark determination on magnetic resonance imaging: a feasibility study. *Clin Oral Investig* 2020;**24**:1339–49.
34. Williams FL, Richtsmeier JT. Comparison of mandibular landmarks from computed tomography and 3D digitizer data. *Clin Anat* 2003;**16**:494–500.
35. Murphy K, van Ginneken B, Klein S, Staring M, de Hoop BJ, Viergever MA, Pluim JPW. Semi-automatic construction of reference standards for evaluation of image registration. *Med Image Anal* 2011;**15**:71–84.
36. Rohlfing T. Image similarity and tissue overlaps as surrogates for image registration accuracy: widely used but unreliable. *IEEE Trans Med Imaging* 2011;**31**:153–63.
37. Kraeima J, Schepers RH, van Ooijen PM, Steenbakkers RJ, Roodenburg JL, Witjes MJ. Integration of oncologic margins in three-dimensional virtual planning for head and neck surgery, including a validation of the software pathway. *J Craniomaxillofac Surg* 2015;**43**:1374–9.
38. Fortunati V, Verhaart RF, Angeloni F, van der Lugt A, Niessen WJ, Veenland JF, Paulides MM, van Walsum T. Feasibility of multimodal deformable registration for head and neck tumor treatment planning. *Int J Radiat Oncol Biol Phys* 2014;**90**:85–93.
39. Leibfarth S, Mönnich D, Welz S, Siegel C, Schwenzer N, Schmidt H, Zips D, Thorwarth D. A strategy for multimodal deformable image registration to integrate PET/MR into radiotherapy treatment planning. *Acta Oncol* 2013;**52**:1353–9.
40. du Bois d'Aische A, De Craene M, Geets X, Grégoire V, Macq B, Warfield SK. Estimation of the deformations induced by articulated bodies: registration of the spinal column. *Biomed Signal Process Control* 2007;**2**:16–24.
41. Webster GJ, Kilgallon J, Ho KF, Rowbottom CG, Slevin NJ, Mackay RI. A novel imaging technique for fusion of high-quality immobilised MR images of the head and neck with CT scans for radiotherapy target delineation. *Br J Radiol* 2009;**82**:497–503.
42. Fortunati V, Verhaart RF, Verduijn GM, van der Lugt A, Angeloni F, Niessen WJ, Veenland JF, Paulides MM, van Walsum T. MRI integration into treatment planning of head and neck tumors: can patient immobilization be avoided? *Radiother Oncol* 2015;**115**:191–4.
43. Egger J, Pfarrkirchner B, Gsaxner C, Lindner L, Schmalstieg D, Wallner J. Fully convolutional mandible segmentation on a valid ground-truth dataset. Proceedings IEEE Engineering in Medicine and Biology Conference (EMBC). *IEEE* 2018:656–60.
44. Wallner J, Schwaiger M, Hochegger K, Gsaxner C, Zemann W, Egger J. A review on multiplatform evaluations of semi-automatic open-source based image segmentation for cranio-maxillofacial surgery. *Comput Methods Programs Biomed* 2019;**182**:105102.
45. Modat M, Ridgway GR, Taylor ZA, Lehmann M, Barnes J, Hawkes DJ, Fox NC, Ourselin S. Fast free-form deformation using graphics processing unitsComput Methods Programs Biomed982010278284. *Comput Methods Programs Biomed* 2010;**98**:278–84.
46. Avants BB, Tustison NJ, Stauffer M, Song G, Wu B, Gee JC. The Insight ToolKit image registration framework. *Front Neuroinform* 2014;**8**:44.
47. van Baar GJ, Forouzanfar T, Liberton NP, Winters HA, Leusink FK. Accuracy of computer-assisted surgery in mandibular reconstruction: a systematic review. *Oral Oncol* 2018;**84**:52–60.

Address:
Stefan Klein
Biomedical Imaging Group Rotterdam
Department of Radiology and Nuclear Medicine
Erasmus University Medical Center
PO Box 2040
3000 CA Rotterdam
The Netherlands
Tel.: +31 10 7043442
E-mail: s.klein@erasmusmc.nl